

Resonating singlet valence plaquettes

S. Pankov

National High Magnetic Field Laboratory, Florida State University, Tallahassee, FL 32306, USA

R. Moessner

Rudolf Peierls Centre for Theoretical Physics, Oxford University, Oxford OX1 3NP, United Kingdom

S. L. Sondhi

*Department of Physics and Princeton Center for Theoretical Physics,
Princeton University, Princeton, New Jersey 08544, USA*

(Dated: November 2, 2018)

We consider the simplest generalizations of the valence bond physics of $SU(2)$ singlets to $SU(N)$ singlets that comprise objects with N sites—these are $SU(N)$ singlet plaquettes with $N = 3$ and $N = 4$ in three spatial dimensions. Specifically, we search for a quantum mechanical liquid of such objects—a resonating singlet valence plaquette phase that generalizes the celebrated resonating valence bond phase for $SU(2)$ spins. We extend the Rokhsar-Kivelson construction of the quantum dimer model to the simplest $SU(4)$ model for valence plaquette dynamics on a cubic lattice. The phase diagram of the resulting quantum plaquette model is analyzed both analytically and numerically. We find that the ground state is solid everywhere, including at the Rokhsar-Kivelson point where the ground state is an equal amplitude sum. By contrast, the equal amplitude sum of $SU(3)$ singlet triangular plaquettes on the face centered cubic lattice is liquid and thus a candidate for describing a resonating single valence plaquette phase, given a suitably defined local Hamiltonian.

I. INTRODUCTION

The physics of valence bonds^{1,2} has provided a fruitful framework for understanding non-Néel phases of $SU(2)$ invariant quantum magnets in low dimensions.^{3,4} In particular, its reformulation as the study of quantum dimer models by Rokhsar and Kivelson⁵ has yielded a sharp but intuitive description of a diverse set of unconventional phenomena, most notably the existence of topologically ordered, fractionalised RVB liquids^{6,7} originally proposed by Anderson and the phenomenon of Cantor deconfinement⁸. Extensions of such dimer models to higher dimensions have been considered^{9,10,11,12,13,14} and in the process the existence of two distinct RVB liquids in $d = 3$ has been demonstrated. The dimer model formulation has the additional virtue of having the manifest interpretation of a strongly coupled, frustrated, gauge theory with RVB phases arising as deconfined phases in such gauge theories.^{15,16} It is also useful to note the recent construction of finite range spin models that realize dimer models arbitrarily accurately in their low energy sectors.^{17,18} We should note that the interest in RVB liquids also comes from a much larger study of topological phases in condensed matter systems.¹⁹

In this paper we pursue a generalization of the valence bond idea to $SU(N)$ groups with $N > 2$ with the aim of searching for topological phases in models with these higher symmetries. The valence bond is replaced by a singlet formed by N spins in the fundamental representation of $SU(N)$. The basic geometrical degrees of freedom thus become triangles for $N = 3$, and objects containing four sites, such as square plaquettes for $N = 4$, and so on. We restrict our study to singlet plaquettes with $N = 3, 4$. With the assumption that for suitable

microscopic Hamiltonians the low energy sector is well described by coverings of the lattice by such objects, we are led to study quantum plaquette models.

These plaquette models are similar in spirit to two-form gauge theories, where degrees of freedom are also defined on plaquettes.²⁰ However, there is one important difference. In the latter, there is a local constraint on plaquettes that share a bond. In our problem, the site origin of the plaquette variables is reflected in their satisfying a site constraint—specifically, that one and only one of the plaquettes that share a common site be occupied by a singlet.

Our strategy in this paper, mirroring that used in the study of valence bond physics, is to begin with a Hilbert space spanned by orthogonal states $|\tilde{\alpha}\rangle$ labelled by admissible plaquette coverings α of the lattice under study. In this space we study the phase diagram of the simplest local Hamiltonian which includes the quantum dynamics of resonance between pairs of plaquettes and a potential energy of interaction between them which we shall term the quantum plaquette model (QPM). As is well known, when the signs of the matrix elements are of the “Perron-Frobenius” form (i.e. no positive off-diagonal matrix elements), such models exhibit a Rokhsar-Kivelson point (which occurs at $v = 2t$ for the case of the cubic lattice, Eq. 4) where the equal amplitude superposition,

$$|\psi\rangle = \sum_{\alpha} |\tilde{\alpha}\rangle \quad (1)$$

saturates a lower bound on the ground state energy of the problem. The diagonal correlations in this state define a classical statistical mechanics of plaquettes which can be studied to establish the true nature of this potentially liquid state. Knowledge of this special point, along

with the analysis of other limits typically allows the phase diagram to be established with some confidence. The remaining challenge is to show that one can actually define a sign convention for wavefunctions of the spins that lead to the desired signs of the matrix elements and finally to construct local spin Hamiltonians that encode all of this physics.

For the $N = 4$ problem on the cubic lattice we report considerable progress on this strategy. We show that matrix elements of the nearest neighbor spin interaction have the desired form. We analyze the statistics of the RK point wavefunction computationally, using a plaquette version of the pocket Monte Carlo algorithm developed for dimers in Ref. 21. We find that the classical system exhibits long range order, in which the preferable plaquette locations form a cubic lattice, analogous to the plaquette valence bond crystal for dimers. This crystalline phase is accounted for analytically from several perspectives. Besides this plaquette phase, the phase diagram of the QPM also contains the staggered and columnar phases and thus the model does not allow a topological phase. By contrast, we find that the equal amplitude sum for the $N = 3$ problem on the face centered cubic (fcc) lattice is liquid and thus a candidate for an RSVP phase. The caveat here arises from the non-ergodic nature of the dynamics in the simplest QPM on this lattice. While we suspect that a longer ranged (but still local) dynamics will fix this, it remains an open problem at this time.

We note that we are, by no means, the first to consider such higher symmetry problems and the emergence of plaquette variables—the new element in our work is the study of QPMs and the idea of the plaquette liquid. In $d = 1$, $SU(4)$ symmetric models are readily constructed by fine-tuning an $SU(2) \times SU(2)$ spin-orbital models,^{22,23,24} or a two-leg ladder.²⁵ In two dimensions, singlet plaquettes have already been considered on a triangular lattice.^{22,26} Separately, $SU(4)$ models have been studied *en route* to connecting large- N $SU(N)$ models with the $SU(2)$ case.^{27,28} The prospect of studying spin-3/2 cold atom systems has inspired an elegant body of work that includes relevant results on $SU(4)$ plaquette solids and even some generalizations to $SU(N)$ ladders^{29,30}. It is also useful to remark here that models with interspersed conjugate representations on bipartite lattices³¹ exhibit singlet dimers (“mesons”) while we consider models with uniform choices of representation which are thus forced to exhibit larger objects (“hadrons”).

This paper is organized as follows. In Sect. II A we repeat Rokhsar and Kivelson’s original “derivation” of the $N = 4$ QPM—essentially, it shows how the appropriate signs can be generated for the matrix elements of the QPM. In Sect. II B we briefly introduce the pocket algorithm and present the results of numerical simulation supporting our view of the ground state at the RK point of the model. In Sect. II C we provide an analytical explanation of the plaquette phase based on a low- and high-dimensional generalisations of the model. In

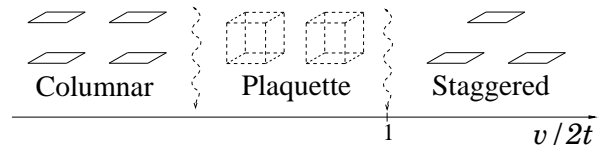


FIG. 1: Minimal phase diagram of the singlet valence plaquette model on a cubic lattice. The transitions are first order.

Sect. III, we present an analysis of the $N = 3$ QPM on the face-centred cubic lattice. In the conclusion, we comment on the model’s utility and open questions.

II. THE $N=4$ QPM ON THE CUBIC LATTICE

A. Microscopics and Hamiltonian

The quantum plaquette model is an effective model for the $SU(4)$ Heisenberg antiferromagnet in a valence plaquette dominated phase, in much the same way the quantum dimer model is an effective model for the $SU(2)$ Heisenberg antiferromagnet in a valence bond dominated phase. As we have noted above, the choice of plaquettes, rather than dimers, as new degrees of freedom is dictated by the fact that in the $SU(4)$ model the lowest energy configuration on a four site lattice is a singlet which mixes equally all four sites.

In this section we will establish some useful properties of the microscopic wavefunctions that correspond to plaquette coverings of the cubic lattice. Should it prove possible to construct a Hamiltonian in the full $SU(N)$ invariant Hilbert space which has the desired coverings, and no other states, as ground states—a non-trivial problem—the results in this section can be used to imitate Refs. 17,18 and rigorously realize the QPM that we introduce here. We will not have much to say about this possibility beyond a few closing remarks in the last section.

A classical plaquette covering of the lattice corresponds to a quantum state, the wave function $|\alpha\rangle$ of which is the product of individual plaquette singlet wave functions. These states are not orthogonal and computing the Hamiltonian matrix elements requires knowledge of the overlap matrix elements. In the case of the dimer model, a simple expression for the overlap matrix elements was given in terms of the length of loops in the transition graph (which is formed by superposing the two dimer coverings under consideration).³²

For the plaquette model, the situation is more involved as the geometry of the transition graph elements is much more complex than the loops formed by the dimers. We have depicted the simplest members in Fig. 2, and it is easy to check that their contribution to the overlap is given by a factor

$$S = 6^{-\frac{l}{2}+1} \quad (2)$$

Here l is the total number of plaquettes in the transition graph element. With this definition of l , the overlap in

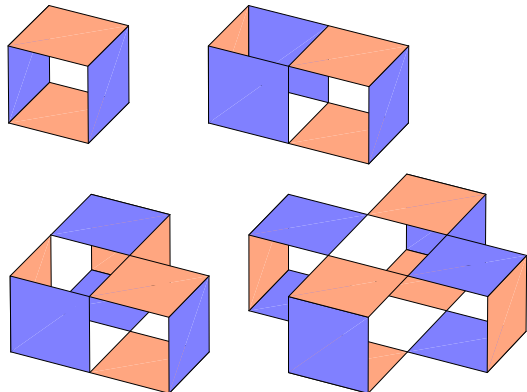


FIG. 2: (color online) Transition graphs with various number of strongly connected parts.

the $SU(2)$ dimer case is given by $2^{-\frac{1}{2}+1}$, which shows that the value of the convergence parameter, $x = 1/6$, is much smaller in the $SU(4)$ case than it is for $SU(2)$, where it equals $1/2$.

In general, configurations contributing to the overlap can be mapped bijectively onto an edge four-coloring model on the graph in which the centres of the plaquettes define the sites and their overlapping corners the edges. For the case of a transition graph element defined by two overlapping checkerboards, one thus finds that the overlap matrix element is even lower, as that entropy³³ implies $.116^{1/2}$. Interestingly, the Pauling estimate for this quantity is the same as for the ice model on the same graph, namely $0.094^{1/2}$, although it is obvious that the entropy of the ice model is lower.

We are not aware of a good rigorous bound for the entropy of such loop models; it is straightforward to show (Appendix B) that $S \leq c \left(3^{1/2}/2\right)^{\frac{1}{2}} = 0.711^{\frac{1}{2}}$, (where c is an unimportant constant) is such a bound, although not at all a strict one. Indeed, all the cases we have explicitly checked have Eq. 2 as an upper bound: $S \leq 6^{-\frac{1}{2}+1}$.

It is convenient to work in the orthogonal basis $|\tilde{\alpha}\rangle$ which can be constructed from the original basis $|\alpha\rangle$ as $|\tilde{\alpha}\rangle = (S^{-\frac{1}{2}})_{\alpha\alpha'}|\alpha'\rangle$, where $S_{\alpha\alpha'} = \langle\alpha|\alpha'\rangle$. Such an orthogonalization can be conveniently carried out analytically assuming the off-diagonal overlap matrix elements to be small.

For example, consider the projection of the nearest neighbor $SU(4)$ Hamiltonian

$$H = \sum_{\langle ij \rangle} \sum_{mn} S_m^n(i) S_n^m(j), \quad (3)$$

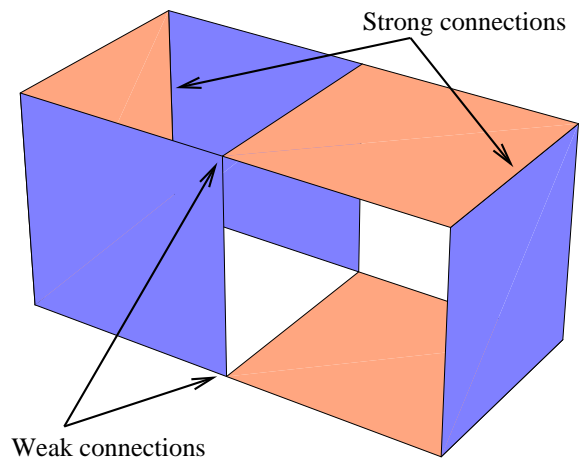


FIG. 3: (color online) Transition graph generated by two configurations (denoted light and dark, respectively) of three plaquettes. A strong connection involves two plaquettes sharing an edge, whereas a weak connection is formed by two plaquettes coinciding at a single site only.

where the S_m^n are $SU(4)$ generators, to the valence plaquette subspace. To this end one expands $S_{\alpha\alpha'}$ or $H_{\tilde{\alpha}\tilde{\alpha}'} = \langle\tilde{\alpha}|H|\tilde{\alpha}'\rangle$ in powers of x . Retaining the leading off-diagonal (kinetic) and diagonal (potential) terms, one obtains the QPM Hamiltonian (also referred to as the RK model):

$$H = -t \sum_{\tilde{\alpha} \neq \tilde{\beta}} |\tilde{\alpha}\rangle \langle \tilde{\beta}| + v \sum_{\tilde{\alpha}} |\tilde{\alpha}\rangle \langle \tilde{\alpha}| \quad (4)$$

where $t = 5x$ and $v = 16x^2$ (see Appendix C for details).

The precise numerical values for t and v should not be taken seriously – due to the presence of higher-order corrections and the absence of other simultaneous perturbations that one can consider, and the choice of plaquette coverings itself remains to be energetically forced. Nonetheless the negative sign of the kinetic term suggests that it is reasonable to study a QPM with the above “Perron-Frobenius” form which is what we will do next. For such models one has the highly useful feature that the ground state is a nodeless wavefunction.

We note that the states $\tilde{\alpha}$ and $\tilde{\beta}$ are connected by a single flip of a pair of plaquettes. It is easy to show that one ground state at the RK point ($v = 2t$) is the equal amplitude superposition of all possible states $|\tilde{\alpha}\rangle$. Studying its properties reduces to sampling (with equal probability) different plaquette coverings. We use a pocket algorithm²¹ to implement this task.

B. Pocket algorithm and MC simulation results

The main advantage of the pocket algorithm is that it efficiently finds possible cluster moves. The cluster moves, starting from a covering A , are constructed as

follows. 1) Consider a transition graph, \mathcal{C} , between A and another covering, B . 2) Pick one connected part of the transition graph, $\mathcal{P} \in \mathcal{C}$; \mathcal{P} is the content of the pocket. 3) Replace the plaquettes of A belonging to \mathcal{P} by those of B . The new covering A' obtained in this way from A is an allowed covering, because it automatically satisfies the close packing constraint.

Finding an uncorrelated new covering B , is of course in general not an easy problem. In the pocket algorithm, it is obtained by acting on A with a symmetry operation³⁴ of the lattice (reflection, for example). Replacing A with a reflected version of itself would of course not yield an independent configuration, but partial replacements (using \mathcal{P} only) eventually do.

This algorithm has been applied to the dimer problem.²¹ In that case the pocket contains a one dimensional object which was shown not to invade space, as loops in dimer transition graphs never branch. The situation is different with plaquettes. It turns out that the transition graph actually percolates and the system is not very close to the percolation threshold. In other words the typical size of non-percolating pocket is small. This, however, does not pose a problem, as the non-percolating pockets contain about 40% of all plaquettes, that is only about 60% of the plaquettes are flipped when the percolating pocket is encountered.

The limiting factor in our case is the quick growth of the equilibration time τ with increasing size of the lattice. The growth appears to be faster than L^3 with L being the size of the lattice. To establish τ we used a binning procedure (see Appendix D for details). Due to these ergodicity restrictions we were limited to a linear size $L = 64$, i.e. a total of $64^3/4 = 65536$ plaquettes, which is sufficient to establish the ordering properties of the model.

In the simulations we measure various (equal time) correlation functions, as a function of plaquette separation. The coordinates $\mathbf{r} = (x, y, z)$ are assigned to a plaquette covering sites (i, j, k, l) according to the rule: $x = \min(x_i, x_j, x_k, x_l)$, $y = \min(y_i, y_j, y_k, y_l)$ and $z = \min(z_i, z_j, z_k, z_l)$, where (x_i, y_i, z_i) are the coordinates of the site i etc. In the same way we can assign coordinates to a flippable pair of plaquettes (which we also call a resonating cube). We use letters X , Y and Z to denote the orientation of the plaquette or the pair forming a ‘resonating cube’. A letter corresponds to the axis orthogonal to a given plaquette (or plaquettes, in case of a resonating cube). Most generally we are interested in studying the correlation function $G_{n\alpha\beta}(\mathbf{r})$, where $n = 1$ for the plaquette correlator, $n = 2$ for the resonating cube correlator, and α and β denote orientations. In fact we will only need to consider the case of $\alpha = \beta$. Using cubic symmetry we drop the orientation index and denote the correlation function as $G_n(r_\perp, r_\parallel)$, where r_\perp and r_\parallel refer to the components of \mathbf{r} orthogonal and parallel to the plaquette.

In Fig. 4, we plot the plaquette correlation function $G_1(0, r)$. It displays oscillations persisting to large separation

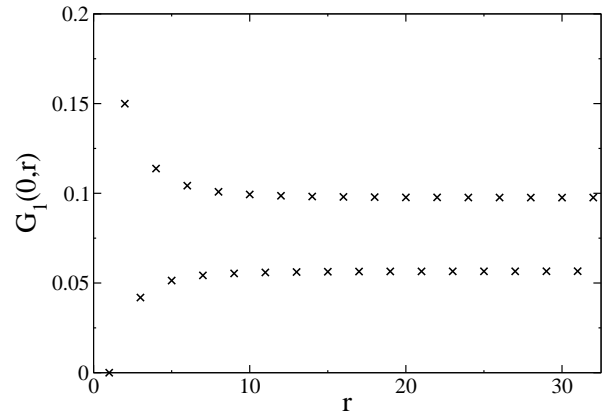


FIG. 4: Correlation function $G_1(0, r)$ for $L = 64$.

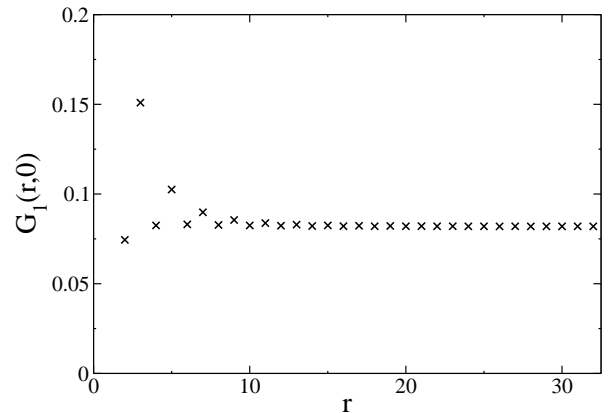


FIG. 5: Correlation function $G_1(r, 0)$ for $L = 64$.

ration r , so that one may conclude that the system possesses long range order. The simplest possibility might be some kind of orientational order (rotational symmetry breaking). Quite a different conclusion may be drawn from the plot of $G_1(r, 0)$, shown in the Fig. 5. At face value, the plot suggests an absence of the long range order, because the oscillations of the correlation functions decrease fast with distance. To detect a possible presence of orientational order we have computed the quantity $\gamma = |\mathbf{n}\mathbf{e}^{(3)}|$, where the components of \mathbf{n} are portions of plaquettes of various orientations and the components of $\mathbf{e}^{(3)}$ are cubic roots of unity. That is $\mathbf{n} = (n_X, n_Y, n_Z)$, $n_X + n_Y + n_Z = 1$ and $\mathbf{e}^{(3)} = (1, e^{i2\pi/3}, e^{i4\pi/3})$. In the case of orientational order, $\langle \gamma \rangle$ would approach a finite value as size of the system increases. In our case it scales to 0 instead.

More insight can be gained from the resonating cube correlation functions. In Fig. 6 we plot the function $G_2(r, 0)$. Unlike the function $G_1(r, 0)$, it clearly captures strong persistent correlations in the direction perpendicular to the plaquette as well. Our findings for G_1 , G_2 and γ can be combined in a coherent picture in which the

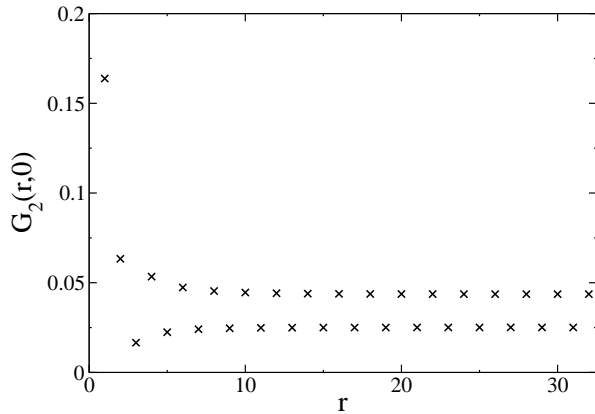


FIG. 6: Pair correlation function $G_2(r, 0)$ for $L = 64$.

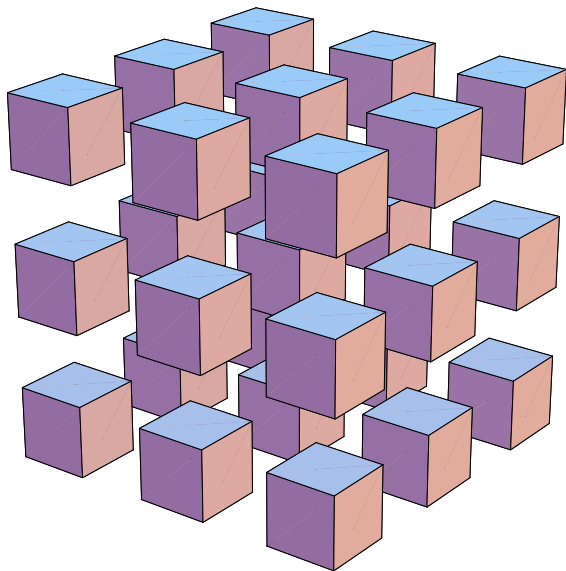


FIG. 7: (color online) Ordering pattern. Plaquettes form resonating cubes which are ordered on a cubic lattice with doubled lattice spacing. Different colors represent plaquettes of three different orientations. The plaquette orientations are uncorrelated over large distances.

resonating cubes form a lattice, breaking translational symmetry, but the orientations of plaquettes on different cubes are not correlated over long distances – thus orientational symmetry is not broken. This is illustrated in Fig. 7.

The presence of long range order (LRO) suggested by Fig. 6 is supported by a scaling analysis. In Fig. 8 we plot differences $\Delta G_2(0, L/2) = G_2(0, L/2 + 1) - G_2(0, L/2)$ and $\Delta G_2(L/2, 0) = G_2(L/2 + 1, 0) - G_2(L/2, 0)$ for $L = 2^p$. We see that ΔG_2 approaches a constant already at $p \sim 5 - 6$. [For larger p , we lose ergodicity, as we show in Appendix D, where we evaluate the relevant equilibration

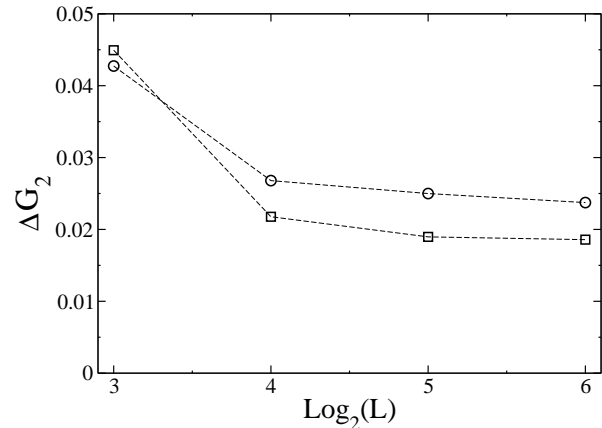


FIG. 8: The curves show scaling of G_2 with the size. $\Delta G_2(0, L/2)$ (circles) and $\Delta G_2(L/2, 0)$ (squares) are plotted vs $\log_2(L)$. Lines are guides to the eye.

time τ using a binning procedure.]

C. Origin of the ordered pattern

Our MC simulations revealed a crystalline phase in the classical system of plaquette coverings of 3D square lattice. The system orders in a cubic lattice pattern with the periodicity equal to two lattice constants of the original lattice.

This ordering is tenuous, as evidenced by the small value of the order parameter. In fact, when one judges a snapshot of the Monte Carlo simulations by eye (Fig. 10), no ordering is evident.

One way to understand the appearance of the long range order is to consider a more general model in which n_d -dimensional hypercubes are arranged on a n_s dimensional lattice. For RSVP, $n_d = n_s = 3$.

Let us start with $n_s = 1$, hypercubes arranged on a chain, Fig. 9. One can then explicitly compute (see details in the Appendix A) the correlation length, which grows as $\sqrt{n_d}$ with n_d . This result can be visualised by noting that a resonating cube can be broken up into two domain walls by fixing the plaquettes to be perpendicular to the chain direction. This costs an entropy $S_d = \ln n_d$. The domain walls can then be separated at will without disturbing other cubes. In a system of length L , this leads to an entropy of $S_w = \ln(\frac{L}{2})$. The correlation length is then determined by the smallest L at which the introduction of domain walls becomes favourable ($S_w > S_d$), which happens at $L = \xi \sim \sqrt{n_d}$.

While there is no true long range order in one dimension, this result shows that the ordering tendency increases with n_d . In this spirit, the case $n_d = n_s = 2$, square dimers, being critical, is indeed already closer to ordering. Zeng and Henley, for the honeycomb lattice,

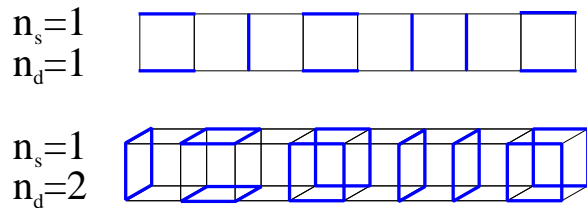


FIG. 9: (color online) n_d dimensional ‘hypercubes’ resonating on a $n_s = 1$ dimensional chain.

have developed a prescription very similar to the introduction of a limit of large n_d for $n_s = 2$, and they found numerically the existence of an ordering transition for sufficiently large n_d .³⁵

Thence, whereas for $n_s = 1$, $n_d \rightarrow \infty$ yields a critical point, $n_s = 2$ requires only a finite n_d to produce ordering. Our results adds the insight that for $n_s = 3$, $n_d = n_s$ is already sufficient to produce ordering.

Some further understanding can be gained by considering higher spatial dimensionality as chains of $d = n_d$ -dimensional hypercubes, transversally coupled in $d - 1$ transverse directions. If a chain and its neighbour (in the \hat{e}_i direction, say) are in registry, a pair of neighbouring resonating cubes can gain further free energy when their plaquettes are perpendicular to \hat{e}_i . This happens in 1 out of d configurations for each cube, and the number of additional states of the two neighbouring plaquettes belonging to different chains resonating together is d . This thus yields an attractive interaction of strength proportional to $1/d$.

For a d dimensional interaction of strength $J \times 1/d$, the critical coupling J would be $O(1)$. Our interaction, however, is amplified by the length of the domains, $\xi \sim \sqrt{d}$, over which individual chains are ordered even in the absence of transverse coupling. This means that for large d , the transversally coupled chains will order. This establishes at least local stability of the plaquette ordering for large d , to which our case $d = 3$ (but not yet the case $d = 2$) is connected.

Note that this ordering pattern does not imply that, even at large d , the plaquettes spend almost all their time resonating with their partner on one given cube. (Such cubes define the ‘site’ of the ordering lattice depicted in Fig. 7). Rather, they spend half of their time resonating on the d bonds emanating from sites of that lattice, as can be seen from an appropriate adaptation of the above argument.

Let p_0 (p_1) be the respective probabilities of finding a crystal site (bond) to be occupied by two parallel plaquettes. The probability of a resonating cube to appear on any given bond is proportional to p_0^2/d^2 . It should be equal to the probability for a resonating cube to leave a bond, which is proportional to p_1/d . In the large d limit other processes are of higher order in $1/d$. Indeed, one can evaluate probability p_i for a resonating cube to appear in locations which are i manhattan steps away

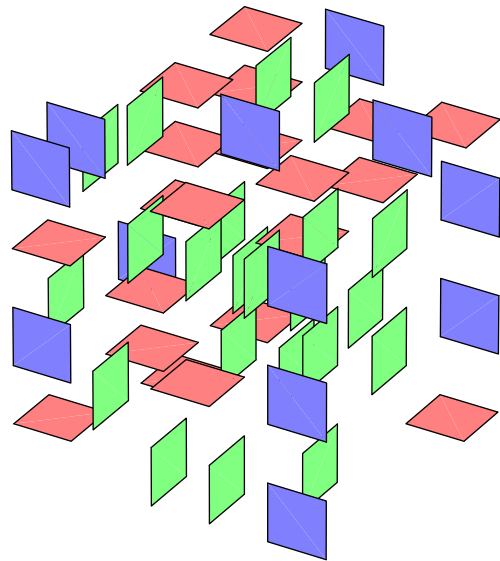


FIG. 10: (color online) Snapshot of a plaquette configuration on a cubic lattice

from crystal sites (manhattan distance here is measured in original lattice spacings, so a bond is one manhattan step away from crystal sites). The relation between p_i and p_{i+1} is similar to the relation between p_0 and p_1 , that is $p_i^2/d^2 \sim p_{i+1}/d$ (as long as $i \ll d$). Therefore $p_i \sim 1/d^{2^i-1}$, while for the number n_i of locations at manhattan distance i we have $n_i \propto d^i$. It follows that only terms with $i = 0, 1$ will contribute in $d \rightarrow \infty$ limit, so a simple relationship holds: $p_1 d = (1 - p_0)/2$. From there we find: $p_0 = 1/2$ and $p_1 = 1/(4d)$.

Because a plaquette is as likely to be found resonating on a bond as it is on a cube, a random snapshot of the cubic lattice will not appear to be ordered, similarly to a snapshot of the face centered cubic (FCC) lattice (Figs.10,11 and Sect. III). A proper analysis reveals, however, that plaquette correlations on the FCC lattice are short range, so the presence of ordering is not a feature of resonating plaquettes in general, but should be attributed to the lack of frustration on the cubic lattice.

D. Phase diagram of the RK model

The above has established that the equal amplitude sum, which has zero energy and thus saturates a lower bound on the ground state energy at the RK point, is crystalline. The QPM Hamiltonian is not ergodic in the full Hilbert space—it moves in topological sectors which we will discuss elsewhere³⁷—and thus will properly exhibit multiple ground states. We can conclude from the simulation of the classical ensemble though, that none of these ground states will be liquid.

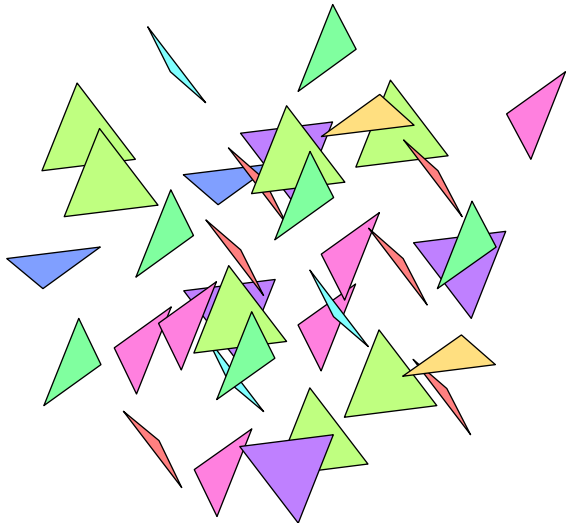


FIG. 11: (color online) Snapshot of a palquette configuration on a FCC lattice. Eight colors are used to represent the different plaquettes, as defined by faces of an octahedron (see Fig.12).

The remainder of the phase diagram of the RK model is completed in the standard way. For $v/t > 2$, any configuration without resonating cubes becomes a ground state. The ordered plaquette phase takes over in a first-order transition at the RK point $v/t = 2$. This is unlike the dimer model, in which there is a moderately exotic deconfined multicritical transition on the square lattice into a solid and into a Coulomb phase on the cubic lattice.^{6,8,16}

For $-v/t \gg 1$, one finds the columnar solid phase, which is unique (up to global symmetry operations) in this case. Whether there are intervening phases between columnar and plaquette solid has not been studied.

III. N=3 QPM ON THE FACE-CENTRED CUBIC LATTICE

To see if the absence of disordered phases is a general feature of such plaquette models, we have also investigated the case of the face-centred cubic lattice. There, the elementary plaquettes are equilateral triangles, the corners of which are defined by a triplet of mutually nearest-neighbour sites. The QPM now includes resonance of a pair of plaquettes the six vertices of which define an octahedron shown in Fig.12.

In Fig. 13, we plot the plaquette correlations of the classical model corresponding to the RK point for various inequivalent combinations of pair orientations and separations in the [011] direction. There are six inequivalent correlation functions for four types of plaquettes

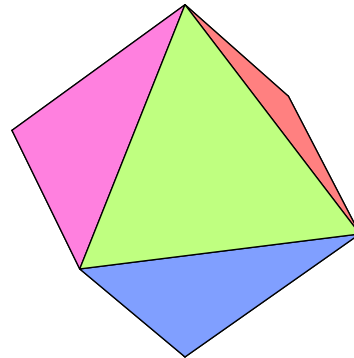


FIG. 12: (color online) Octahedron defining the plaquette types on the FCC lattice.

adjacent at an octahedron vertex. All correlators decay with distance to the value given by uncorrelated plaquettes. This decay is a rapid exponential, with correlation lengths of less than a lattice spacing, ranging from ~ 0.3 (diagonal component) to ~ 0.7 (off-diagonal component) of nearest neighbor distances.

This demonstrates that a classical hard-core plaquette model is in a strongly disordered phase and we would be tempted to conclude, by standard arguments, that we have identified a point in an RSVP phase that sits at a first order transition to a staggered crystal. The connection of the classical sum to the RK point of the QPM, however, is more complicated than in the case of the cubic lattice. The plaquette pair flip is very constrained and by itself breaks up the Hilbert space into a very large number of largely frozen states with local quantum fluctuations so that it is only the sum of these individual states that exhibits liquidity. It seems very likely that the inclusion of resonance dynamics on larger clusters will remove this pathology and establish the RSVP state. However, at present we are unable to explicitly solve this problem.

IV. CONCLUDING REMARKS

Can the above quantum plaquette models be realised in experiment? Conceivably, they can arise in the case of low energy Ising degrees of freedom which reside on the midpoints of plaquettes of a lattice, and which obey the appropriate hardcore constraint. Their simplest quantum dynamics would then be that of a QPM.

Regarding our original motivation of finding degrees of

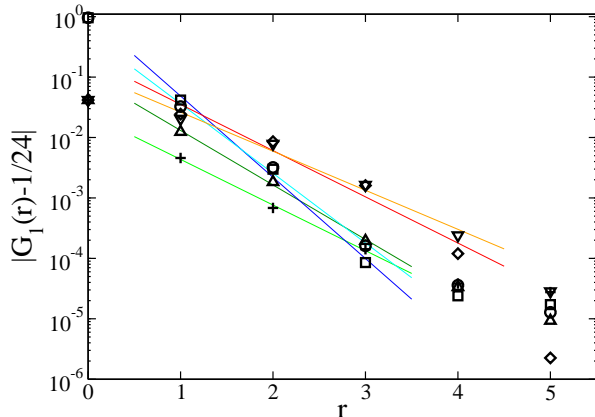


FIG. 13: (color online) Connected part of the correlation function $G_1(r)$ for various plaquette orientations on the FCC lattice. The distance r is measured in units of the nearest neighbor distance.

freedom with a native $SU(N)$ symmetry, we first observe that following initial work on dimer ground state ensembles of Klein models³⁶, there now exist prescriptions for local $SU(2)$ invariant Hamiltonians which produce RK quantum dimer models in a controlled fashion.^{17,18,38}

However, no simple generalisation of Klein models for $SU(4)$ models with plaquette ground states is known yet, in part for the reason that was pointed out in Ref. 36 for dimers on the square lattice. There, the projectors occurring in the Hamiltonian allow ground states containing not only dimers on nearest neighbour but also on next nearest neighbour bonds. In an analogous manner, for $SU(4)$ plaquette ground states, we are also lead to other (e.g. non-planar) units of four spins forming a singlet. Actually realising an $SU(4)$ degree of freedom is of course also no trivial matter in $d > 1$, as combining an orbital pseudospin 1/2 degree of freedom with an $SU(2)$ to form an $SU(4)$ invariant Hamiltonian requires a fine-tuning of interaction parameters which is not immediately suggested by the natural symmetries of orbitals making up the pseudospin 1/2. Similarly, whether or not there exist lattice models realising an $SU(3)$ QPM on the face-centred cubic lattice that exhibits an RSVP phase is left for further investigation.

It is worth noting that $SU(4)$ spins do of course not present the exclusive entry point to plaquette degrees of freedom. We have already referred to work on spin-3/2 $SU(2)$ systems that give rise to plaquettes^{29,30}. One can also consider that in the same sense in which dimers can be thought of as low-energy composite degrees of freedom consisting of a pair of resonating $SU(2)$ spins with $S = 1/2$, a plaquette might be considered as a composite of a pair of resonating dimers. There is thus nothing fundamentally untoward about resonating valence plaquettes – this view being reinforced by the findings of Ref. 26, who found plaquette ordering with the same $\sqrt{12} \times \sqrt{12}$ supercell proposed for resonating dimers on

the same lattice.^{39,40} Similarly, attractive interactions in the simple cubic dimer model lead to an ordered phase, albeit one with columnar order,⁴¹ rather than the plaquette order observed here.

Finally, our work on the RK point also provides an entry to the study of classical hard plaquettes in $d > 2$. In particular, the topological and ergodicity properties of these models should present an interesting topic for further research.

Acknowledgements

We thank B. Douçot, D. Huse, W. Krauth, F. Mila, M. Mostovoy, K. Penc and M. Troyer for useful discussions. We are very grateful to W. Krauth for collaboration on closely related work. This work was supported in part by the Ministère de la Recherche with an ACI grant. Most of it was undertaken at Laboratoire de Physique Théorique de l'Ecole Normale Supérieure, CNRS-UMR 8549.

APPENDIX A: PLAQUETTES ON THE CHAIN

We use the transfer matrix method to compute correlation function of d dimensional plaquettes on a chain. Each plaquette can assume d orientational states: one orthogonal to the direction of the chain and $d - 1$ parallel. We write the Hamiltonian as $H = \sum_i H_{i,i+1}$ and compute the transfer matrix $T_i^{\alpha\alpha'} = \langle \alpha | \exp(-\beta H_{i,i+1}) | \alpha' \rangle$, where $|\alpha\rangle$ represents local degrees of freedom. Provided the Hamiltonian is translationally invariant the correlation function $C(x) = \langle M_i M_{i+x} \rangle$ of some operator M can be written as:

$$C(x) = \frac{\text{Tr} M T^x M T^{N-x}}{\text{Tr} T^N} \quad (\text{A1})$$

where N is the length of the chain (periodic boundary conditions are assumed). In the thermodynamic limit $N \rightarrow \infty$ we have:

$$C(x) = \sum_{\alpha} \langle \lambda_0 | M | \lambda_{\alpha} \rangle \langle \lambda_{\alpha} | M | \lambda_0 \rangle \left(\frac{\lambda_{\alpha}}{\lambda_0} \right)^x \quad (\text{A2})$$

where $|\lambda_{\alpha}\rangle$ are eigenstates of the transfer matrix and λ_0 is its largest (in absolute value) eigenvalue. The asymptotic form of the connected part of the correlation function is determined by the next largest eigenvalue $\tilde{\lambda}$ such that $\langle \lambda_0 | M | \tilde{\lambda} \rangle \langle \tilde{\lambda} | M | \lambda_0 \rangle \neq 0$, so that the correlation length is given by $\xi = 1 / \ln |\lambda_0 / \tilde{\lambda}|$. In our case all states are degenerate, so the transfer matrix is simply proportional to $2d - 1$ dimensional matrix of the following form:

$$T = \begin{pmatrix} 1 & A & 0 \\ 0 & 0 & E \\ B & C & 0 \end{pmatrix} \quad (\text{A3})$$

where E is $(d-1) \times (d-1)$ identity matrix, and all the matrix elements of A , B and C are equal 1. The matrix C is $(d-1) \times (d-1)$ square matrix, while A and B are $1 \times (d-1)$ and $(d-1) \times 1$ matrices respectively. It is not hard to find that T has only two nonzero eigenvalues:

$$\lambda = 1/2 \pm \sqrt{d-3/4} \quad (\text{A4})$$

from where we find $\tilde{\lambda}/\lambda_0 = -1 + 1/\sqrt{d} + O(1/d)$. The first term encodes the fact that the connected part of the correlation function oscillates, while the second term determines the correlation length $\xi = \sqrt{d}$.

APPENDIX B: OVERLAP MATRIX ELEMENT

In the fundamental representation four basis states (flavors) are used to represent an $SU(4)$ spin. The invariance of the $SU(4)$ singlet plaquette wave function under rotations in spin space dictates the singlet to be a fully antisymmetrized combination of all four flavors on four sites:

$$|\psi_s\rangle = \frac{1}{\sqrt{24}} \sum_{P\{1234\}} (-1)^p |1234\rangle \quad (\text{B1})$$

where the four flavors $\{1234\}$ are permuted in all possible ways and p is the parity of permutation P . In each term there is one flavor per site, that is flavors are permuted among different sites. The prescription for fixing overall sign of the wave function will be given below. We consider lattice states which are products of singlet wave functions corresponding to each plaquette. We need to compute the overlap matrix element between two such states. It can be visualized with the help of the transition graph - the graph which is made of all partially overlapping plaquettes. Only those have to be included, as the fully overlapping plaquettes multiply the matrix element by 1. The total overlap matrix element is a product of overlap matrix elements corresponding to disconnected parts of the transition graph, therefore it is sufficient to consider only a connected transition graph.

Two plaquettes can be connected either via a common edge or a single common site. We call these strong and weak connections, respectively. The common edge in the strong connection is called connecting edge, and the common sites in weak connections are called connecting sites. If it is possible to connect two plaquettes by a path belonging to the transition graph and going through strong connections only, then two plaquettes are said to belong to the same strongly connected part. Using the fact that each site in the transition graph is shared by exactly two plaquettes, it is easy to check that either the strongly connected part has exactly four weak connections attached, or it has no weak connections and we call it a simple graph.

Each plaquette in the transition graph corresponds to a certain term $|1234\rangle$ of the singlet wave function. The overlap is non zero only when sites shared by different

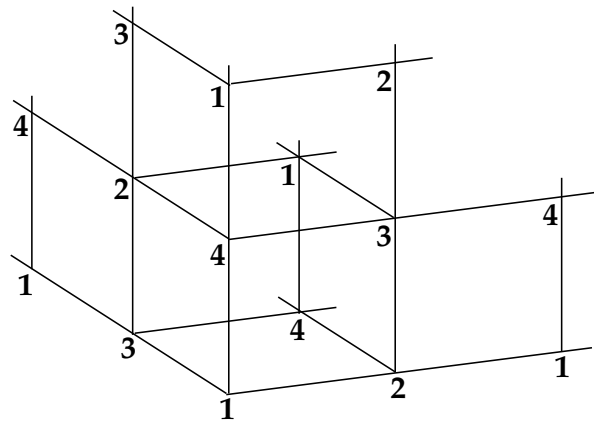


FIG. 14: Assignment of flavors which respects the constraint of no two sites in a plaquette carrying same flavor.

plaquettes carry identical flavors in each of the two plaquettes. Thus a nonzero overlap is parameterized by assigning a flavor per site in the transition graph, under the constraint that no two sites in a plaquette carry the same flavor. This is always possible to do by assigning flavors to all sites of the lattice in the following way : assign 1 to the point $(0, 0, 0)$, 2 to the point $(1, 0, 0)$, 3 to the point $(0, 1, 0)$, 4 to the point $(0, 0, 1)$ and then translate this configuration by $(\pm 1, \pm 1, \pm 1)$ to cover all sites of the lattice (see Fig. 14). It is easy to check that any plaquette on the lattice contains four different flavors.

It has to be decided how to choose signs for plaquette singlet wave functions to ensure that the overlap matrix elements of the initial and final state of a resonance process are positive. It is straightforward to check that it is enough to require the term $|1234\rangle$ in each singlet wave function, whose flavors coincide with our prescription, to be positive.

The assignment of flavors to the sites in the transition graph is not unique. This is most easily seen by making a connection between this assignment and a loop model, which in turn establishes the link to the four-colouring model mentioned in the text. We partition the sites in the graph (for a given allowed assignment of flavors) in the following way. Connect sites with flavors 1 and 2 which belong to the same plaquette. Do the same with the sites carrying flavors 3 and 4. In this way, all sites will be divided into noncrossing loops. Notice that in each loop two flavors can be exchanged without violating the constraint. The configurations of flavors which can be connected by a sequence of such transformations are said to belong to the same loop decomposition.⁴² The number of such configurations is 2^{n_l} , where n_l is the number of loops in the decomposition. Some loops contain weak connections, while others do not - we call them nonlocal and local loops, respectively. From the flavor constraint (any plaquette includes all four flavors) it follows that a nonlocal loop goes through at least two strongly connected parts and has at least length $l = 4$, while a local loop belongs to a single strongly connected part and has

length $l = 2$. Obviously, $n_l = n_{ll} + n_{nl}$, where n_{ll} and n_{nl} is the number of local and nonlocal loops correspondingly. Taking into consideration that $n_{nl} \leq n_s$ and $n_{ll}^i \leq l_i - 1$, where n_{ll}^i and l_i are the number of local loops and the number of plaquettes in the i th strongly connected part (the case $n_s = 1$ is not included here), we can write the following inequality for the contribution \tilde{S} to the overlap matrix element from a given loop decomposition:

$$\frac{1}{6}\tilde{S} = \left(\frac{1}{24}\right)^{\frac{l}{2}} 2^{n_l} \leq 6^{-\frac{l}{2}} \quad (\text{B2})$$

The prefactor of $1/6$ accounts for various ways of distributing four flavors among two classes of loops. Notice that for a simple graph $n_{ll} = l$ and $n_{nl} = 0 < 1 = n_s$, so the above result still holds in that case, with the inequality turning into an equality.

In the next step we derive a bound on the number of loop decompositions. For the sake of compactness we use terms ‘‘vertex’’ and ‘‘connection’’ in place of ‘‘strongly connected part’’ and ‘‘weak connection’’ below. Four connections belonging to the same vertex are joined by nonlocal loops. This can be done in three different ways. Therefore there are at most 3^{n_s} loop decompositions. Clearly, not all decompositions are allowed, because for two nonlocal loops going through the same vertex (there are at most two such loops) a choice of flavors of one of the loops uniquely determines flavors of the second loop. This restriction can be formulated as a problem of coloring loops with just two colors, let us say black and white. We start with no nonlocal loops defined, that is all connections disjointed and not colored. We will be joining four connections (belonging to the same vertex) at a time, and color them according to the way they are joined. Without loss of generality, we choose to do the joining procedure on those vertices which already have colored connections.

In this way colors are always defined uniquely (apart from the first step). It is easy to check that there are at most three ways to join connections when none or one of them has been colored. There are at most two ways of joining connections when two of them have been colored. There is at most one way of joining, when three or all connections have been colored. Thus the upper bound on the number M of loop decomposition can be written as:

$$M = \max \left\{ 2^{n_s} \left(\frac{3}{2}\right)^{n_0+n_1} \left(\frac{1}{2}\right)^{n_3+n_4} \right\} \quad (\text{B3})$$

with the following constraints imposed

$$\begin{aligned} \sum_{i=0}^{i=4} n_i &= n_s \\ \sum_{i=0}^{i=4} i n_i &= 2n_s \end{aligned} \quad (\text{B4})$$

where n_i is the number of vertices which undergo the joining procedure having i colored connections, and thus is positive. From Eq. B4 we have $2n_0 + n_1 = n_3 + 2n_4$, so the maximum in Eq. B3 is achieved when n_0 and n_3 are minimized, while n_1 and n_4 are maximized. In the best case $n_1/2 = n_4 = n_s/3$, and $M(n_s) = 3^{2n_s/3}$. Since $n_s \leq l$, the bound for S equals the bound for \tilde{S} times $M(l)$:

$$S \leq 6 \left(\frac{3^{\frac{1}{3}}}{2}\right)^{\frac{l}{2}} \quad (\text{B5})$$

APPENDIX C: MATRIX ELEMENT COMPUTATIONS FOR SU(4) QPM

We use $|\tilde{\alpha}\rangle$ notations for the orthonormal states and $|\alpha\rangle$ for the original states. We only need to consider states which differ by orientation of a single pair of plaquettes, we thus name the states according to the orientation of the pair in the YZ, ZX and XY planes as $|X\rangle$, $|Y\rangle$ and $|Z\rangle$. We first compute matrix elements $\langle\alpha|H|\beta\rangle$. It is easy to check that:

$$H_{ij}|\alpha(ijkl)\rangle = -|\alpha(ijkl)\rangle \quad (\text{C1})$$

where $H_{ij} = \sum_{mn} S_m^n(i)S_n^m(j)$ is the part of the Hamiltonian acting on the bond (ij) . The location of the plaquette is explicitly shown in $|\alpha(ijkl)\rangle$ and S_m^n are $SU(4)$ generators.²² In the fermionic representation $S_m^n = a_m^\dagger a_n$, so $S_m^n|\mu\rangle = \delta_{n\mu}|m\rangle$ where μ is the flavor. The term $S_m^n(i)S_n^m(j)$ simply exchanges flavors m and n on sites i and j from where the Eq.(C1) follows. We note that only H_{ij} with i and j belonging to any of the two plaquettes need to be considered. When $\alpha \neq \beta$ there is always a plaquette containing both i and j , therefore for any bond $\langle\alpha|H_{ij}|\beta\rangle = -x$ and $\langle\alpha|H|\beta\rangle = -12x$ because twelve bonds belong to the pair of plaquettes. When $\alpha = \beta$ only eight bonds belong to an individual plaquette, these bonds give $\langle\alpha|H_{ij}|\alpha\rangle = -1$. For a bond shared by the plaquettes one can estimate $\langle\alpha|H_{ij}|\alpha\rangle = \sum_{\beta \neq \alpha} |\langle\alpha|\beta\rangle|^2 \langle\beta|H_{ij}|\beta\rangle = -2x^2$. So we have $\langle\alpha|H|\alpha\rangle = -8 - 8x^2$.

Let us compute, for example, $\langle\tilde{X}|H|\tilde{X}\rangle$ and $\langle\tilde{X}|H|\tilde{Y}\rangle$. To the lowest order $|\tilde{X}\rangle = |X\rangle - \frac{x}{2}(|Y\rangle + |Z\rangle)$ and $|\tilde{Y}\rangle = |Y\rangle - \frac{x}{2}(|X\rangle + |Z\rangle)$. Then $\langle\tilde{X}|H|\tilde{X}\rangle = \langle X|H|X\rangle - \frac{x}{2}(\langle X|H|Y\rangle + \langle X|H|Z\rangle + h.c.) + \dots = -8 + 16x^2 + \mathcal{O}(x^3)$. The constant term -8 is actually independent of plaquette configuration and can thus be dropped. For the off diagonal element we find $\langle\tilde{X}|H|\tilde{Y}\rangle = \langle X|H|Y\rangle - \frac{x}{2}(\langle X|H|X\rangle + \langle Y|H|Y\rangle) + \dots = -5x + \mathcal{O}(x^2)$. Thus we obtain for the kinetic and potential term in the RK Hamiltonian $t = 5x$ and $v = 16x^2$.

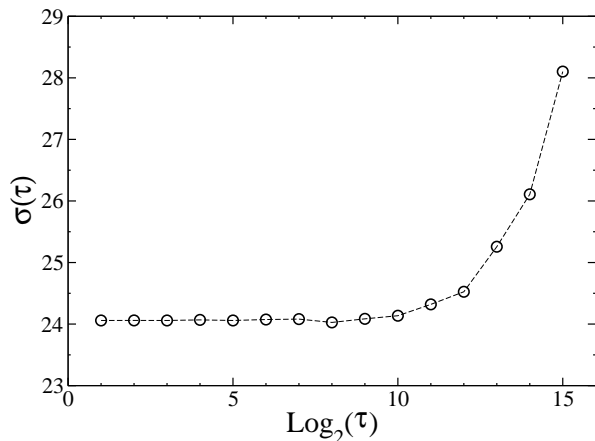


FIG. 15: The standard deviation $\sigma(\tau)$ of $\langle G(0, L/2) \rangle_\tau$ plotted vs $\text{Log}_2\tau$ for $L = 48$.

TABLE I: Equilibration time

L	8	16	32	64
τ	$2^4 = 16$	$2^7 = 128$	$2^{11} = 2048$	$\geq 2^{15} = 32768$

APPENDIX D: DETERMINATION OF THE EQUILIBRATION TIME

The error of statistically independent measurement decreases with the number of measurements n as $n^{-\frac{1}{2}}$. If,

however, the measurements are not independent, the error cannot be reduced beyond certain limit, as more measurements do not add any new information. This allows to estimate correlation time corresponding to some physical quantity O by measuring fluctuation of the average value $\langle O \rangle_\tau$ computed over the time span τ . More precisely, we measure $\langle O \rangle_\tau$ over m successive intervals of time of length τ . From m average values we compute the standard deviation $\sigma(\tau)$ of the distribution of $\langle O \rangle_\tau$. In the same run we can measure $\langle O \rangle_{\tau/2}$ in $2m$ time intervals by subdividing each τ interval in two. The corresponding standard deviation $\sigma(\tau/2)$ is thus computed from $2m$ measurements. The procedure of subdivision (of creating smaller bins, hence the term binning) can be continued as far as needed. By plotting $\sigma(\tau)$ vs $\text{Log}_2\tau$ we estimate the equilibration time τ_{eq} as the time where $\sigma(\tau)$ stops changing as τ is lowered. Alternatively, one could keep the number m of intervals fixed, while decreasing the number of measurements in each interval, by doubling the timing between successive measurements τ . Again, the standard deviation $\sigma(\tau)$ would depend on τ only for $\tau > \tau_{eq}$. This is shown in Fig. 15, where we plotted $\sigma(\tau)$ for $L = 48$, for the correlation function $G(0, L/2)$. The equilibration time can be estimated to be $\tau_{eq} \sim 2^{14}$. The equilibration times estimated in this way for other sizes are summarized in the Table I.

-
- ¹ P. Fazekas and P. W. Anderson, *Philos. Mag.* **30**, 23 (1974)
- ² P. W. Anderson, *Science* **235**, 1196 (1987)
- ³ S. Sachdev in “Quantum magnetism”, U. Schollwöck, J. Richter, D. J. J. Farnell and R. A. Bishop eds, (Springer, Berlin, 2004)
- ⁴ G. Misguich and C. Lhuillier in “Frustrated spin systems”, H. T. Diep ed., (World-Scientific, Singapore, 2005)
- ⁵ D. S. Rokhsar and S. A. Kivelson, *Phys. Rev. Lett.* **61**, 2376 (1988)
- ⁶ R. Moessner and S. L. Sondhi, *Phys. Rev. Lett.* **86**, 1881 (2001)
- ⁷ G. Misguich, D. Serban and V. Pasquier, *Phys. Rev. Lett.* **89**, 137202 (2003).
- ⁸ E. Fradkin, D. A. Huse, R. Moessner, V. Oganesyan and S. L. Sondhi, *Phys. Rev. B* **69**, 224415 (2004); A. Vishwanath, L. Balents, T. Senthil, *Phys. Rev. B* **69**, 224416 (2004)
- ⁹ D. A. Huse, W. Krauth, R. Moessner, and S. L. Sondhi *Phys. Rev. Lett.* **91**, 167004 (2003)
- ¹⁰ M. Hermele, M. P. A. Fisher, and L. Balents *Phys. Rev. B* **69**, 064404 (2004)
- ¹¹ C. L. Henley *Phys. Rev. B* **71**, 014424 (2005)
- ¹² O. I. Motrunich and T. Senthil *Phys. Rev. B* **71**, 125102 (2005)
- ¹³ C. Xu, *Phys. Rev. B* **74**, 224433 (2006)
- ¹⁴ A. Seidel, H. Fu, D.-H. Lee, J. M. Leinaas and J. Moore, *Phys. Rev. Lett.* **95**, 266405 (2005)
- ¹⁵ E. Fradkin and S. A. Kivelson, *Mod. Phys. Lett. B* **4**, 225 (1990)
- ¹⁶ R. Moessner, S.L. Sondhi, and Eduardo Fradkin, *Phys. Rev. B* **65**, 024504 (2002)
- ¹⁷ K. S. Raman, R. Moessner and S. L. Sondhi, *Phys. Rev. B* **72**, 064413 (2005)
- ¹⁸ S. Fujimoto, *Phys. Rev. B* **72**, 024429 (2005)
- ¹⁹ X.-G. Wen, “Quantum Field Theory Of Many-body Systems” (Oxford University Press, Oxford, 2004).
- ²⁰ R. Savit, *Rev. Mod. Phys.* **52**, 453 (1980).
- ²¹ W. Krauth and R. Moessner, *Phys. Rev. B* **67**, 064503 (2003)
- ²² Y. Q. Li, M. Ma, D. N. Shi and F. C. Zhang, *Phys. Rev. Lett.* **81**, 3527 (1998)
- ²³ Y. Yamashita, N. Shibata, and K. Ueda, *Phys. Rev. B* **58**, 9114 (1998)
- ²⁴ M. van den Bossche, P. Azaria, P. Lecheminant and F. Mila *Phys. Rev. Lett.* **86**, 4124 (2001)
- ²⁵ T. Hikihara, T. Momoi, and X. Hu, *Phys. Rev. Lett.* **90**, 087204 (2003)
- ²⁶ K. Penc, M. Mambrini, P. Fazekas and F. Mila *Phys. Rev. B* **68**, 012408 (2003)
- ²⁷ F. F. Assaad, *Phys. Rev. B* **71**, 075103 (2005)
- ²⁸ A. Paramekanti and J. B. Marston, *J. Phys. Cond. Matt.* **19**, 125215 (2007)
- ²⁹ C. Wu, *Mod. Phys. Lett. B* **20**, 1707 (2006)
- ³⁰ S. Chen, C. Wu, S.-C. Zhang, and Y. Wang, *Phys. Rev. B* **72**, 214428 (2005)

- ³¹ N. Read and S. Sachdev, Nucl. Phys. B **316**, 609 (1989)
- ³² B. Sutherland, Phys. Rev. B **37**, 3786 (1988)
- ³³ J. L. Jacobsen and J. Kondev, Nucl. Phys. B **532**, 635 (1998).
- ³⁴ C. Dress and W. Krauth, J. Phys. A **28**, L597 (1995).
- ³⁵ C. Zeng and C. L. Henley, Phys. Rev. B **55**, 14935 (1997)
- ³⁶ J. Chayes, L. Chayes and S. A. Kivelson, Commun. Math Phys. **123**, 53 (1989)
- ³⁷ S. Pankov et al., *work in progress*.
- ³⁸ Z. Nussinov, arXiv:cond-mat/0606075; Z. Nussinov and G. Ortiz, arXiv:cond-mat/0702377.
- ³⁹ R. Moessner and S. L. Sondhi, Phys. Rev. B **63**, 224401 (2001)
- ⁴⁰ R. Moessner, S. L. Sondhi and P. Chandra, Phys. Rev. Lett. **84**, 4457 (2000)
- ⁴¹ F. Alet, G. Misguich, V. Pasquier, R. Moessner and J. L. Jacobsen, Phys. Rev. Lett. **97**, 030403 (2006)
- ⁴² Any two colour configurations connected by a sequence of such loop moves contribute to the overlap with the same sign. It may however be the case that some topological sectors of the four-colouring model cannot be connected by such loop moves. This would, if anything, suppress the overlap for larger transition graph elements.